Modelling the diurnal cycle of tropical convection across the "Grey Zone"

Article

Accepted Version

It is advisable to refer to the publisher's version if you intend to cite from the work. See Guidance on citing.

CentAUR

Central Archive at the University of Reading

Reading's research outputs online
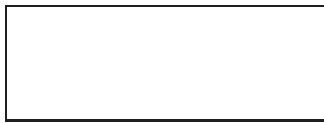
Modelling The Diurnal Cycle of Tropical Convection Across the "Grey Zone"

K. J. Pearson,[a]*G. M. S. Lister,[a] C. E. Birch,[b] R. P. Allan,[a] R. J. Hogan[c] and S. J. Woolnough[a]

[a]*NCAS, Department of Meteorology, University of Reading, Reading, UK.*

[b]*Institute for Climate and Atmospheric Science, School of Earth and Environment, University of Leeds, Leeds, UK.*

[c]*Department of Meteorology, University of Reading, Reading, UK.*

*Correspondence to: Environmental Systems Science Centre, Harry Pitt Building, University of Reading, Reading, RG6 6AL. E-mail: k.j.pearson@reading.ac.uk

We present the results of simulations carried out with the Met Office Unified Model at 12 km, 4 km and 1.5 km resolution for a large region centred on West Africa using several different representations of the convection processes. These span the range of resolutions from much coarser than the size of the convection processes to the cloud-system resolving and thus encompass the intermediate "grey-zone". The diurnal cycle in the extent of convective regions in the models is tested against observations from the Geostationary Earth Radiation Budget instrument on Meteosat-8. By this measure, the two best-performing simulations are a 12 km model without convective parametrization, using Smagorinsky style sub-grid scale mixing in all three dimensions and a 1.5 km simulations with two-dimensional Smagorinsky mixing. Of these, the 12 km model produces a better match to the magnitude of the total cloud fraction but the 1.5 km results in better timing for its peak value. The results suggest that the previously-reported improvement in the representation of the diurnal cycle of convective organisation in the 4 km model compared to the standard 12 km configuration is principally a result of the convection scheme employed rather than the improved resolution *per se*. The details of and implications for high-resolution model simulations are discussed. Copyright ⓒ 2013 Royal Meteorological Society

1. Introduction

The processes involved in tropical weather patterns span a large range of temporal and spatial scales from individual convection cells through mesoscale convective systems to superclusters that interact with regional and global circulatory patterns such as African Easterly Waves and the Madden Julian Oscillation (Leary and Houze 1979; Machado *et al.* 1993). Until recently, limitations in computer power made capturing both the small-scale processes and large circulatory patterns in the same simulation, with the consequent requirement for both high resolution and a large domain, prohibitively expensive. As a result, both routine operational numerical weather prediction and long-term climate simulations have generally been carried out at spatial resolutions that require the parametrization of the small-scale processes like convection.

The tendency of the parametrized approach to produce convection too early in the day is well known (e.g. Yang and Slingo 2001). Several studies (e.g. Guichard *et al.* 2004; Grabowski *et al.* 2006; Hohenegger *et al.* 2008) have demonstrated how cloud system resolving simulations with

resolutions of a few kilometers and explicit representation of the convection process can resolve the timing problem. Improving the representation of convection for models that operate at lower resolution is clearly important for both operational forecasting and climate prediction. In particular, errors in the diurnal cycle of cloud cover in climate models affect their radiative balance. Cloud feedbacks are the largest uncertainties in climate sensitivity estimates (Randall *et al.* 2007). Stratton and Stirling (2012) used results of a study of entrainment and detrainment rates from idealised cloud resolving models (Stirling and Stratton 2012) to modify the parametrization in the Met Office climate model, resulting in an improved amplitude and timing of precipitation. Kendon *et al.* (2012) found that a high resolution (1.5 km) model simulation was better able to represent the diurnal cycle and intensity distribution of precipitation over the U.K. than a 12 km resolution simulation (using parametrized convection). It is vital that understanding and modelling of the interaction between contrasting scales are tested by evaluating large-domain simulations, with resolution sufficiently high to be cloud-system resolving, against available observations.

In a previous paper (Pearson *et al.* 2010), we described a new technique for assessing the diurnal development of tropical convection, illustrated by early results from the Cascade project of simulations using the Met Office Unified Model (UM) over a West Africa region. These were run at 12 km and 4 km resolution, employing a parametrization scheme and explicitly resolving the convection, respectively. These highlighted how the standard parametrized convection scheme in the UM also fails to reproduce the observed evolution of the size of convective region as well as the timing. In this paper, we revisit this case study with the full set of model configurations and assess their respective ability to reproduce the diurnal cycle of cloud organisation.

2. Method

The overall model configuration was as described in Pearson *et al.* (2010) based on that used by Lean *et al.* (2008) who tested the implications for convection over the UK. The UM version 7.1 (Davies *et al.* 2005) was run as a Local Area Model over a West Africa test region at 3 different resolutions (approximately 12 km, 4 km and 1.5 km) and with a variety of representations of the convection process. The models were one-way nested inside a run from the next coarser domain that provided the initial state and lateral boundary conditions. The 12 km simulations were initialised using analysis fields from the European Centre for Medium-Range Weather Forecasts and updates to the models were subsequently applied solely through the lateral boundary conditions. As a result, the simulations did not run in a "forecast" mode but were still guided by the large-scale circulatory environment. Any comparison with observation must, therefore, be carried out statistically. The domains are plotted in Figure 1. All the domains used a rotated coordinate system with the North pole at [180°W,79°N]. The details are summarised in Table I.

Convection was represented either through a parametrization scheme or allowed to occur explicitly. The parametrized model used a Gregory-Rowntree scheme (Gregory and Rowntree 1990) with closure based on the convectively available potential energy (CAPE) and a
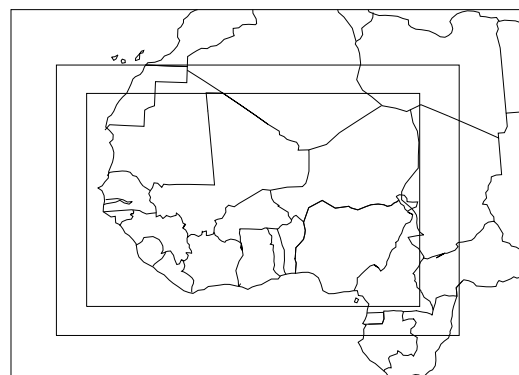

Figure 1. The nested computational domains used by the 12 km, 4 km and 1.5 km resolution models.

Table I. Summary of the different domains used by the models. $N_{x,y}$ are the number of grid boxes in the relevant direction, $\Delta_{x,y}$ is the grid spacing and Lon_0 and Lat_0 are the coordinates of the lower left corner in the rotated system.

Resolution	N_x	N_y	$\Delta_{x,y}$	Lon_0	Lat_0
12 km	460	340	0.11°	-25.0	-15.0
4 km	1110	776	0.036°	-21.0	-11.0
1.5 km	2444	1630	0.0135°	-18.0	-8.0

relaxation timescale of 30 mins. Vertical subgrid mixing occurred in the boundary layer scheme but there was no horizontal subgrid mixing. The "explicit" models at all resolutions retained the parametrization scheme but now restricted with a relaxation time asymptoting to 20 mins at zero CAPE but increasing sharply with increasing CAPE. Combined with a retuned parameter set this led the scheme to generate negligible increments from mid- and deep-level convection and left only a small residual effect representing shallow convection. Typically the "explicit" models produced less than 1% of their rainfall from this residual convection scheme compared to 95% in the parametrized case. Models that eliminate the scheme entirely produce similar results overall but have a greater number of instances of grid-scale storms with unrealistically high rainfall (Roberts 2003). The models using explicitly resolved convection employed two different methods for sub-gridscale mixing. The 2D scheme used the standard boundary layer scheme for vertical mixing and a Smagorinsky-type mixing in the horizontal direction whereas the 3D scheme made use of Smagorinsky mixing in all three dimensions. These are described more fully below.

The model uses a terrain-following hybrid height coordinate (η) that is decribed in detail in Davies *et al.* (2005). This runs from zero at the top of any orography to unity at a selected height above mean sea level. Model levels are spaced quadratically in η at low levels up until a suitable level where the surfaces become flat and thicken more quickly. For the models with 38 vertical levels, the vertical grid spacing was ~ 300 m at 1 km and ~ 900 m at 10 km. With 70 levels the vertical spacing was ~ 100 m at 1 km and ~ 500 m at 10 km.

In common with many other models, diffusion is applied to the potential temperature, moisture and wind fields when the convection is explicitly resolved. Although the UM does not require this for stability, it does prevent cells collapsing to the grid-scale (Lean *et al.* 2008). The diffusion takes place in two stages. The vertical component (if the 3D scheme is selected) utilises the implicit solver in the boundary layer scheme but now applied to the whole atmosphere with a suitable value for the coefficients as outlined below. The 2D (horizontal) component is calculated explicitly and takes place along layers of η. The diffusion coefficients are set by the viscosity (ν) that is applied to vector quantities or the diffusivity (ν_h) applied to scalar quantities. The diffusion and Lagrangian interpolation methods are discussed in detail in Staniforth (2006).

The classical Smagorinsky-Lilly approach calculates the viscosity (ν) from the modulus of the strain tensor ($S_{ij} = \frac{\partial u_i}{\partial x_j} + \frac{\partial u_j}{\partial x_i}$) via

$$\nu = (c_S \Delta)^2 \frac{||S_{ij}||}{\sqrt{2}} = \lambda_0^2 \left(\sum \frac{S_{ij}^2}{2} \right)^{\frac{1}{2}} \quad (1)$$

where Δ is the grid spacing and c_S is generally treated as a constant.

The implementation in the UM differs in two ways as set out in Halliwell (2007) and Lock (2007). First, the mixing length is reduced close to the surface by

$$\frac{1}{\lambda} = \frac{1}{\lambda_0^2} + \frac{1}{[k(z+z_0)]^2} \quad (2)$$

where z is the height above the surface, z_0 is the roughness length of the surface and $k \approx 0.4$ is the von Karman constant. The second difference is the adjustment of the coefficients by stability functions (f_m, f_h), such that

$$\nu = \lambda^2 \frac{||S_{ij}||}{\sqrt{2}} f_m(Ri) \quad (3)$$

$$\nu_h = \lambda^2 \frac{||S_{ij}||}{\sqrt{2}} f_h(Ri) \quad (4)$$

where Ri is the local Richardson number. The stability functions take the form

$$f_X(Ri) = \begin{cases} 1 - \frac{g_0 Ri}{1 + D_X \psi |Ri|^{\frac{1}{2}}} & Ri < 0 \\ 1 - 0.5 g_0 Ri & 0 < Ri < 0.1 \\ (2.0 g_0 Ri)^{-1} & Ri > 0.1 \end{cases} \quad (5)$$

where the subscript X refers to either m or h, g_0 and D_X are constants and ψ is the ratio of "neutral mixing lengths" as defined in Lock (2007). The quantity ψ will always take the value of unity in the 3D case and only differ in the 2D case where there is a significant contribution to turbulence in the boundary layer from subgrid orography or vegetation.

Being the least computationally expensive to run, the 12 km models were run with the largest number of configurations. Four models were run with 38 vertical levels. One used the parametrized convection scheme and three used explicitly represented convection with subgrid mixing modelled by: 2D Smagorinsky mixing, 3D Smagorinsky mixing and 3D Smagorinsky mixing with the

mixing factor (c_S) halved. A fifth 12 km model was run with the 3D mixing scheme and 70 vertical levels.

The parameter settings for the sub-grid mixing in the 12 km models were the same as for the 4 km models where they were optimised for operational use over the UK. The 1.5 km resolution model had a separate set of optimised parameters. It is not clear *a priori* how these ought to be modified to account for the coarser resolution of the 12 km models. In the limit of poor resolution, it may be more appropriate to fix λ_0 instead of c_S (Halliwell 2007). Hence, the reduction of a factor 2 in c_S might be regarded as partial compensation for the reduced resolution of the 12 km model.

The 4 km model was run with both 2D and 3D mixing schemes. Running the model with the 2D scheme at 1.5 km resolution generated instabilities that caused the code to crash. Therefore, options were selected to invoke a more sophisticated treatment of the vertical advection of potential temperature. This has the effect *inter alia* of improving the representation of gravity waves. The settings are not used routinely since to run stably they require a shorter timestep with attendant computation cost. The same options were applied to a further 4 km run with the 2D mixing scheme. The 1.5 km model calculated increments from shortwave (SW) and longwave (LW) radiative heating every 5 mins as opposed to every 15 mins for the other simulations. These model configurations are summarised in Table II.

Each simulation, with one exception, was run for 10 model days. Neglecting the first day of each to allow for "spin-up" resulted in data covering 26 July to 3 Aug 2006 inclusive. The exception was the 1.5 km simulation which ended a day earlier.

Observational data for comparison to the models was provided by the Geostationary Earth Radiation Budget (GERB) instrument, a broadband radiometer onboard Meteosat-8 with a standard nadir resolution of 50 km (Harries *et al.* 2005). However, we used higher resolution (~ 10 km) outgoing longwave radiation (OLR) data available every 15 min through combination with the Spinning Enhanced Visible and Infrared Imager (SEVIRI): the NRT V003 ARCH product (Dewitte *et al.* 2008). The same 9 day period was analysed as for the models.

In Pearson *et al.* (2010), we introduced a method for comparing the diurnal cycle of convective activity using OLR. Cloud pixels are identified in a scene on the basis of an upper threshold OLR flux value, regions of contiguous pixels located and their area (A) calculated. Histograms of the number of systems in lengthscale bins ($L_{i,\text{edge}} = \sqrt{A_i} = 2^{2+i/4}$ km for $i = 0, 1, 2 \ldots$) are generated for each image. These are normalised using the mean and standard deviation of the number of systems (N) over time at each lengthscale to generate the standard score statistic

$$Z(L, t) = \frac{N(L, t) - \bar{N}(L)}{\sigma(L)}. \quad (6)$$

This is then plotted as a grey scale time series to give a representation of the anomaly in the number of systems at a particular lengthscale as a function of time.

The above aproach has the advantage of requiring the model to produce a quantity (OLR) that is directly comparable to observations available across the whole domain at high time resolution and which we can use to test the development of convective organisation. It does so

Model Number	1	2	3	4	5	6	7	8	9
Resolution (km)	12	12	12	12	12	4	4	4	1.5
Vertical Levels	38	38	38	38	70	70	70	70	70
Mixing Scheme	None	2D	3D	3D	3D	2D	3D	2D	2D
Timestep (mins)	5	2.5	2.5	2.5	2.5	1	1	0.5	0.25
Smagorinsky constant (c_S)		0.1	0.1	0.05	0.1	0.1	0.1	0.1	0.2
Extra feature	Param. conv.			$c_S/2$				θ adv.	θ adv.

at the expense of moving us a step away from variables that are directly related to the underlying convection processes but which are limited in their temporal and spatial coverage. These underlying processes are being addressed in other parts of the project (*eg.* Marsham *et al.* 2011; Holloway *et al.* 2012)

It is possible to conduct a similar analysis using a lower bound on the rainfall rate as a criterion for a site of convection. However, we are hampered in this approach by the lack of a directly comparable observational dataset. An attempt to apply this to the 3 hourly Tropical Rainfall Measuring Mission data product 3B42 for this region and time period yielded no discernible signal.

3. Results

The diurnal cycles of all 10 datasets are compared in Figure 2 with a temporal resolution of 15 min and using an upper OLR threshold of $150\,\mathrm{W\,m^{-2}}$. All the datasets were rebinned to the same 12 km spatial resolution before the flux threshold was applied and the results were repeated for a second day.

The observed GERB data (panel f) shows that the peak number of systems for small sizes occurs in mid-afternoon and then gradually later in the day as the size increases. Beyond a lengthscale of about 200 km the absolute number of systems is small and the diurnal signal is lost. Systems of all sizes up to this limit persist until around midnight but appear relatively rare thereafter.

3.1. Parametrized Convection

Panel a in Figure 2 demonstrates how the parametrization scheme in the UM triggers convection symmetrically in time about noon with lengthscales up to around 100 km beginning and ending together. Rather than organised activity, this results from the decision making process that initiates convection occurring independently in each grid column. The range of lengthscales reflects that of the regions over which similar meteorological conditions prevail for the variables going into that decision. As a result of the lack of communication between columns, size evolution does not occur and systems neither grow individually nor aggregate.

A similar comparison using a *lower* threshold total precipitation rate of $10^{-5}\,\mathrm{kg\,m^{-2}\,s^{-1}}$ is shown in Figure 3. The total rainfall rate was only available at hourly intervals for the 12 km models but at 15 min resolution for the other model runs. The parametrized approach results in a sharp peak in the number of rainy grid cells with again no apparent size evolution.

3.2. Explicitly Resolved Convection with 2D Smagorinsky Mixing

Panels b and g of Figure 2 contain the results from the two simulations with 2D Smagorinsky mixing at 12 km and 4 km resolutions respectively. Both show that allowing the simulations to explicitly model convection results in an improved timing of onset of cloud generation. The evolution from small to large systems also occurs at a rate similar to those shown by observations. The improved behaviour of the 4 km over the 12 km model reported in Pearson *et al.* (2010) is thus principally a result of the convection scheme employed and not due to the improved resolution.

The clearest deficiency in these models is the way in which some large systems break up suddenly by "shattering" into small pieces (as discussed in Pearson *et al.* 2010). These are so numerous that they dominate the small systems that are generated at the onset of convection around 1400 UTC. Examining the absolute number of systems in each size bin shows that a (now) secondary peak does still occur at this time. Figure 3 reveals that the "breakup" cloud has negligible associated rain. In this figure, generated using a rainfall rate threshold, all 3 resolutions using the 2D subgrid mixing show an elegant evolution from small- to large-scale organisation in a similar way to the development indicated by the observed OLR. However, as we are rather comparing apples and oranges in this case, such similarity is merely encouraging rather than definitive.

As mentioned previously, the initial attempt to run the UM at 1.5 km resolution using the 2D Smagorinsky scheme as configured in the coarser resolution models led to numerical instabilities. These manifested as strong vertical velocities with a regular alternating "chequerboard" pattern. Similar behaviour appears to occur in the region of the subset of systems in the 4 km model that "shatter". Here we also see strong but less extreme downdraughts. While these are also less regularly arranged, there are a spiderweb network of contiguous pixels with large negative values of vertical velocity.

Animations of OLR for the 1.5 km and 4 km models with the revised settings for potential temperature advection show no sign of the "shattering". However, panels i and j of Figure 2 show that both do still generate too many systems at small scales when the systems dissipate. This may imply that while systems dissipate correctly into fragments with a range of sizes, they are still doing so in a shorter time window than reality. The GERB data shows a background number of small systems throughout the second half of the day.
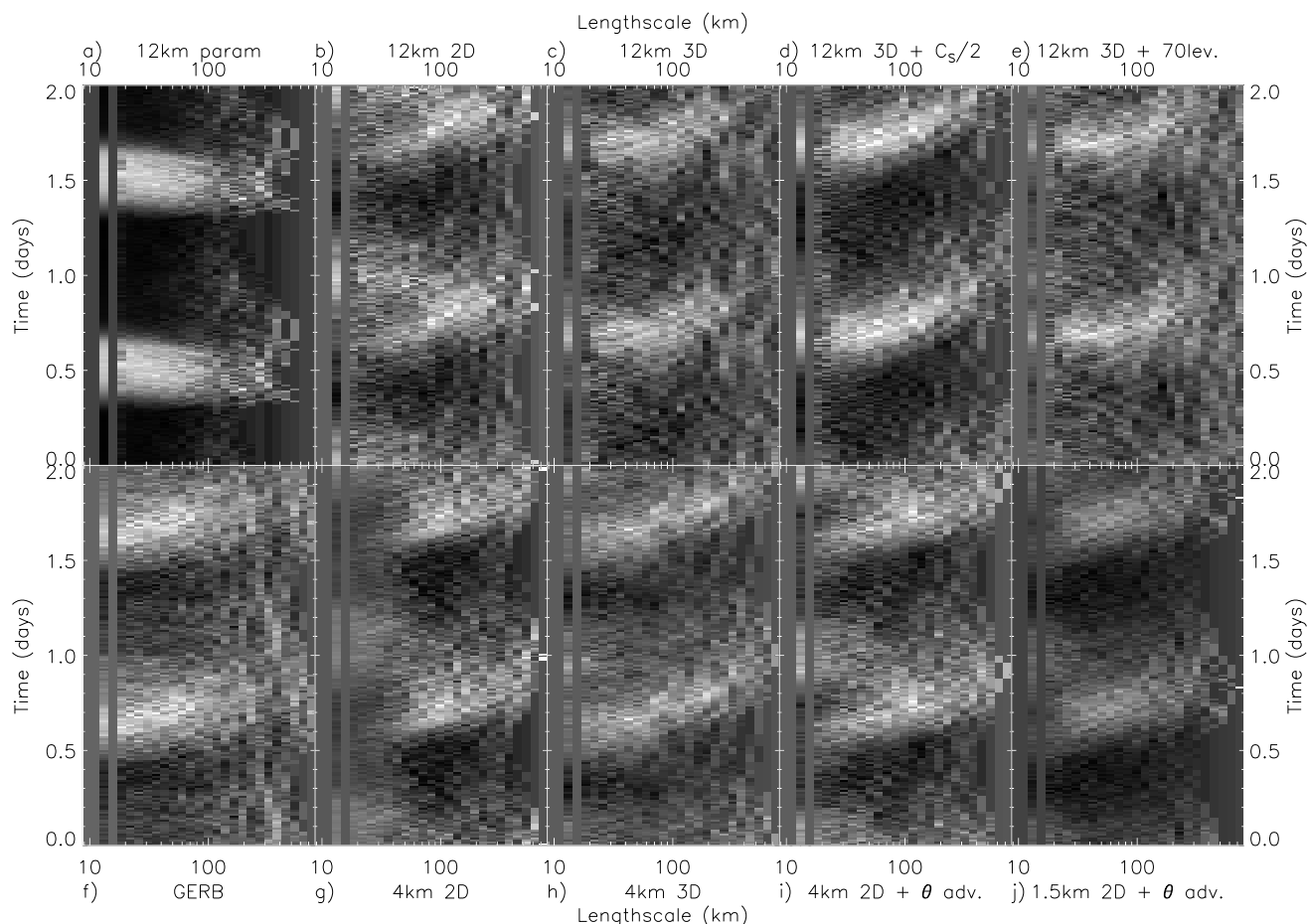
Figure 2. Comparison of the diurnal cycle of cloud using equation (6) based on an OLR threshold of 150 W m^{-2} for all 10 datasets. From left, top row: models 1-5 from Table II, bottom row: observational GERB data, models 6-9. The greyscale range on each panel is set independently. Light shading indicates more systems at that time than the mean for that lengthscale, dark shading less systems than the mean.

3.3. Explicitly Resolved Convection with 3D Smagorinsky Mixing

Panels c and h of Figure 2 show the results from two runs carried out using a 3D Smagorinsky mixing scheme at 12 km and 4 km resolution. Neither shows any evidence for the unphysical breakup that occurred with the 2D models. However, the 12 km models do exhibit unwelcome behaviour not apparent here with a runaway secular increase in the total cloud fraction in the domain. A further 12 km resolution model was run that increased the number of model levels to 70 to match that of the 4 km. This produced very similar results (panel e) to the 38 model level run (panel c) with a clear diurnal cycle but also a steadily increasing cloud fraction. It proved possible to resolve this issue, however, by reducing the mixing length parameter and the results plotted in panel d still show a clear diurnal cycle. Examining it critically, it does still lacks any "background" systems at small sizes and runs out to longer lengthscale systems than the observed data.

3.4. Overall Comparison

Table III gives the values of linear correlation coefficient for each of the model standard score maps plotted in Figure 2 against that from the GERB data. The closest models to the data (with $r=0.65$) are the 1.5 km model and the

Table III. Correlation coefficient r for each of the standard score maps from the model datasets in Figure 2 against that from the observed GERB data.

Model	r
1	0.03
2	0.41
3	0.57
4	0.65
5	0.54
6	0.33
7	0.61
8	0.51
9	0.65

12 km model with 3D mixing and reduced mixing length parameter. The 4 km model with 3D mixing is the next best, ahead of the initial 12 km model run that used 3D mixing. This latter result highlights that although this method of presenting the data accentuates the diurnal evolution of storm sizes, it does not account for the absolute amount of cloud which for this model became runaway.

The mean diurnal variation in the fraction of the scene identified as cloud, is plotted in Figure 4 for the four model datasets with the highest value of r excluding those
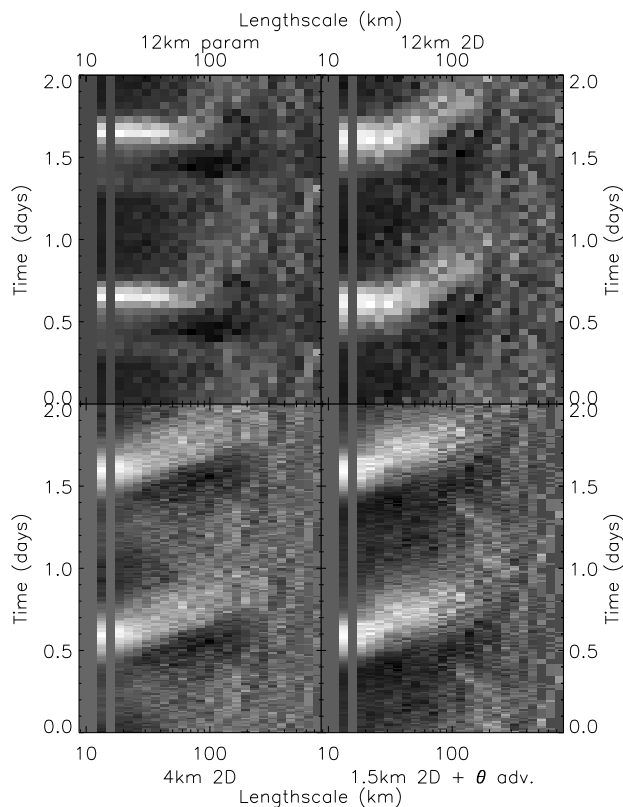
Figure 3. Comparison of the diurnal cycle, via the total precipitation rate, for the 12 km model using parametrized convection (model 1, top left) and models at 12 km, 4 km and 1.5 km resolution that use the 2D Smagorinsky mixing scheme: models 2 (top right), 6 (bottom left) and 9 (bottom right) respectively.

Figure 4. Comparison of the mean diurnal cloud fraction for 5 of the datasets: GERB (solid lines, plus symbols) and models 4 (dotted, asterisk), 7 (dashed, diamond), 8 (dot-dashed, triangles) and 9 (triple-dot-dashed, squares). Symbols are only plotted every 10 data points.

Figure 5. Comparison the time of peak for the diurnal component of cloudiness at each lengthscale for 5 of the datasets: GERB (solid lines, plus symbols) and models 4 (dotted, asterisk), 7 (dashed, diamond), 8 (dot-dashed, triangles) and 9 (triple-dot-dashed, squares).

with erroneous runaway cloud generation (models 3 and 5). The slight discontinuities that are apparent across midnight result from small absolute differences between the start and end of each dataset that are not completely smoothed out given the relatively small number of days in the sample. The model simulation with the best representation of the amplitude of the diurnal cycle is the 12 km model with 3D mixing and reduced mixing length. The 4 km models and 1.5 km model on this figure show slightly improved timing for maximum cloud cover but significantly larger values of cloud fraction. By taking the Fourier transform in time for each lengthscale we can identify the time of the peak in the diurnal cycle of cloudiness. This is plotted in Figure 5. The 12 km and 4 km models that use the 3D mixing scheme appear to stay close to the observed GERB data. The behaviour at short lengthscales for the other explicit models is affected by the overproduction of systems in the breakup phase.

In the above analysis, we have been principally interested in testing the relative merits of the reproduction of convective organisation by the models. It is possible, however, that the models might be producing improved results in this respect while diverging wildly in their representation of the underlying processes. As a check on their reasonableness in this regard, Figs 6 and 7 show mean vertical profiles above Niamey for the potential temperature and relative humidity respectively. Also plotted are the mean observed profiles with a shaded error representing the standard error on the mean. These observations come from radiosonde measurements made at 6-hourly
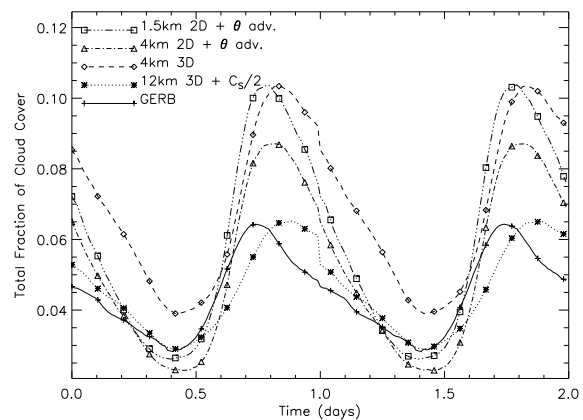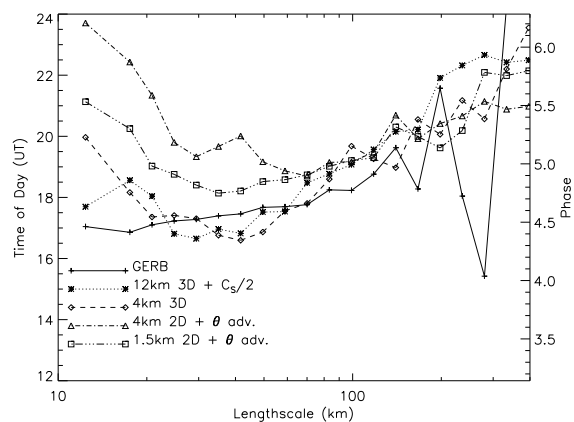
intervals over the 9 days which occurred during a Special Observation Period conducted as part of the African Monsoon Multidisciplinary Analysis (AMMA, Parker *et al.* 2008). The rms error of all the models with respect to the observations are summarised in Table IV.

We should be cautious in overinterpreting these profiles: the models are not running in a forecast mode and the selected station may happen not to be representative of the simulation as a whole. Nonetheless, of the 4 best diurnal cycle models the potential temperature profile of the 12km model with reduced 3D mixing (model 4) is noticeably closer to the observations at 00Z and 18Z, particularly in the lowest few kilometres. At 06Z and 12Z the profile is somewhat flatter but the overall error is comparable to the other models. The relative humidity profiles of model number 4 again compare well to the other models at 00Z and 18Z although some of the structure in the lower atmosphere appears to be missed. However, the performance at 06Z and 12Z is slightly poorer than the other models.

4. Conclusion

Previous studies have noted the improved representation of the diurnal cycle of clouds and precipitation on moving
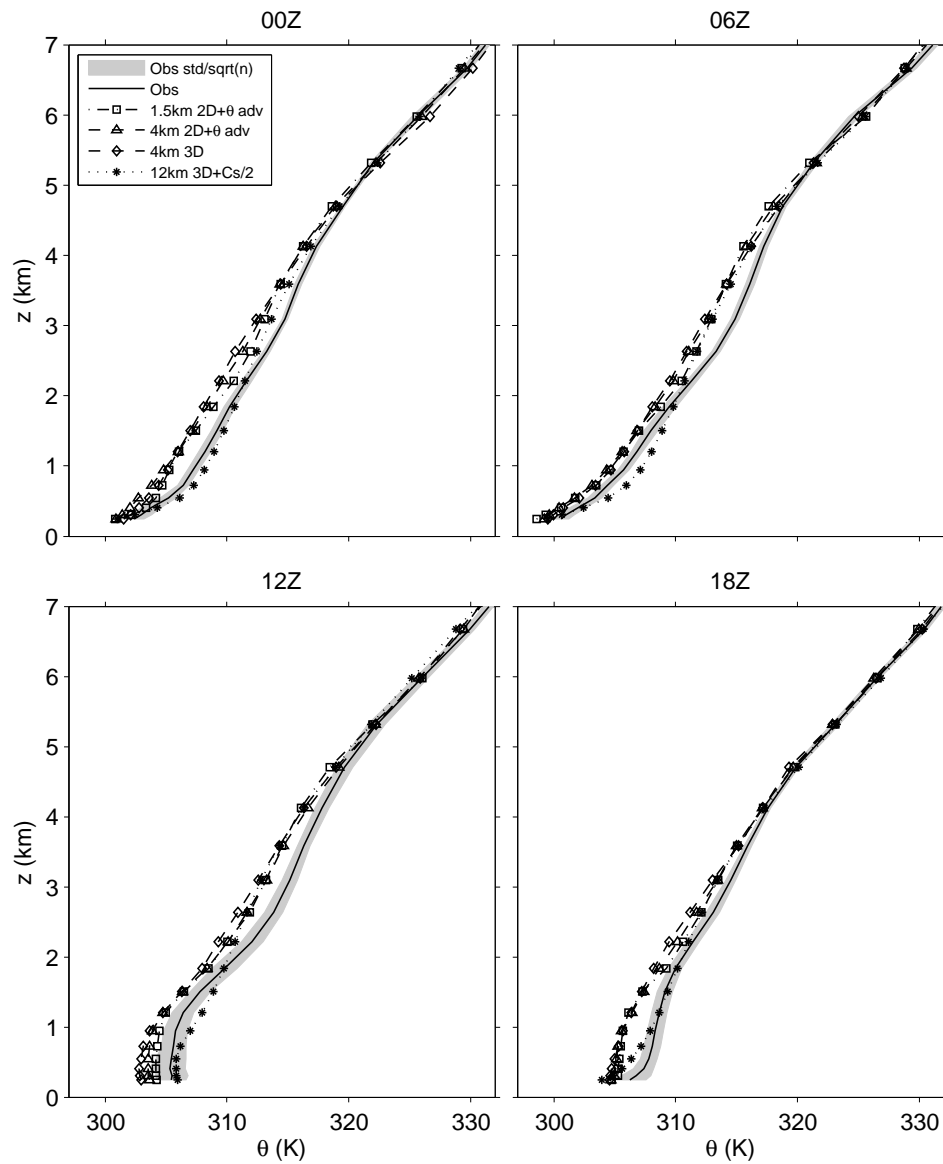
Figure 6. Comparison of the mean vertical profile of potential temperature above Niamey for 4 of the models: 4 (dotted, asterisk), 7 (dashed, diamond), 8 (dashed, triangles) and 9 (dot-dashed, squares). Also plotted is the observed mean profile (solid) with shading representing the standard error on the mean.

Table IV. Root mean square error between each of the models and observations for the potential temperature (θ) and relative humidity mean profiles up to 12 km above Niamey at the indicated times.

Model	θ (K)					Relative Humidity				
	00Z	06Z	12Z	18Z	All	00Z	06Z	12Z	18Z	All
1	2.29	2.14	1.95	2.30	4.35	10.13	11.45	10.11	13.62	22.83
2	1.73	1.70	1.87	1.97	3.64	11.13	11.40	8.13	15.06	23.38
3	1.45	1.80	1.86	1.59	3.36	14.96	15.45	17.32	14.99	31.42
4	1.68	1.92	2.09	1.88	3.79	9.99	11.88	12.68	9.79	22.31
5	1.73	2.37	1.64	1.42	3.65	18.98	17.65	17.69	14.46	34.55
6	1.28	1.31	1.44	1.49	2.76	9.91	8.98	5.38	11.78	18.61
7	1.95	1.84	2.32	2.18	4.16	10.69	8.13	11.95	9.16	20.18
8	1.94	1.77	2.04	1.96	3.86	11.95	9.04	11.08	11.91	22.12
9	1.77	1.79	1.94	1.92	3.71	9.39	8.95	8.74	12.12	19.79

to higher spatial resolutions (e.g. Pearson *et al.* 2010; Kendon *et al.* 2012). We find that, in our case study over Africa, the improvement in the development and growth of convective organisation is principally the result of
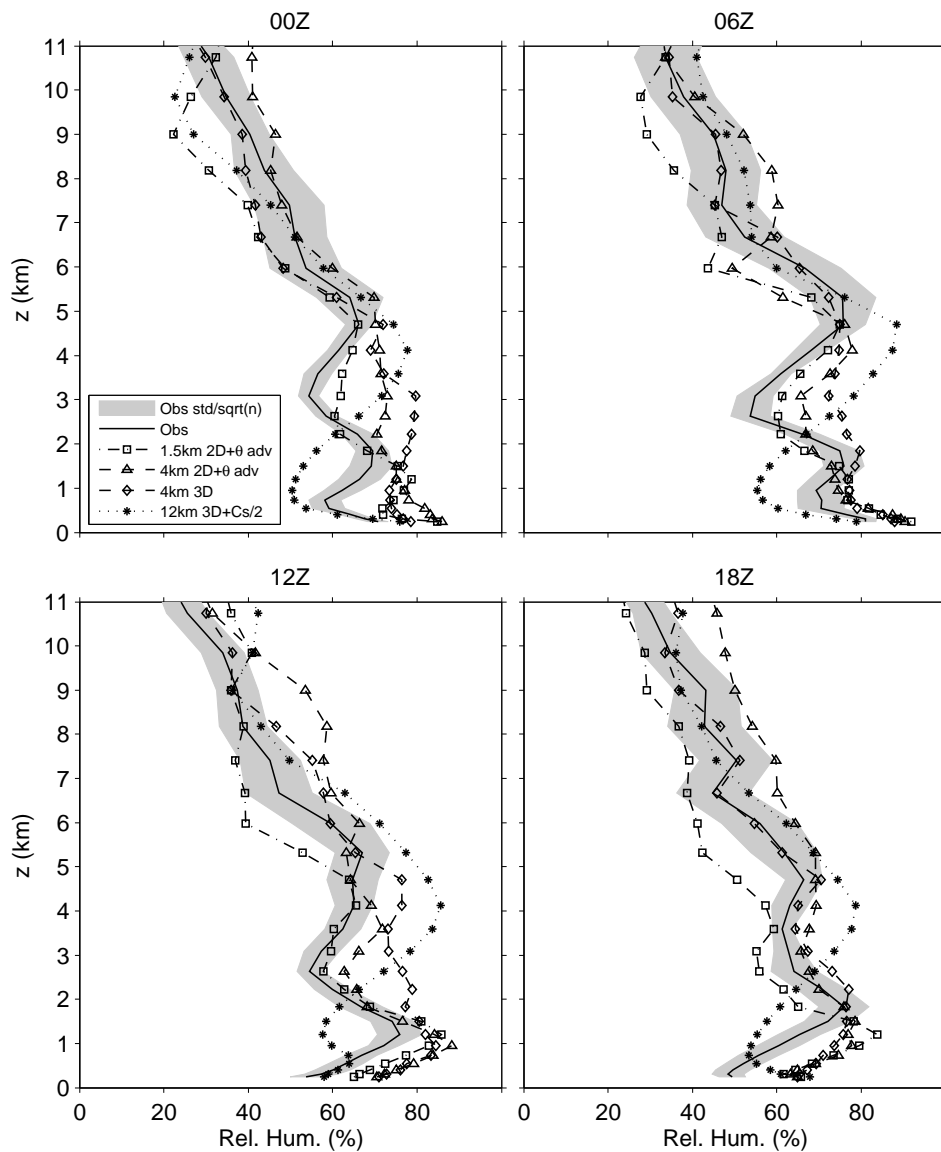
Figure 7. Comparison of the mean vertical profile of relative humidity above Niamey for 4 of the models: 4 (dotted, asterisk), 7 (dashed, diamond), 8 (dashed, triangles) and 9 (dot-dashed, squares). Also plotted is the observed mean profile (solid) with shading representing the standard error on the mean.

the parametrization employed at coarser resolution and the mechanism for representing convection rather than the increase in resolution itself. The two best-performing models in terms of diurnal storm-size evolution were a 1.5 km resolution model with 2D subgrid mixing and a 12 km resolution model with 3D mixing. Remarkably, the resolution of the 12 km model is at least an order of magnitude coarser than the resolutions normally regarded as sufficient to explicitly simulate deep convection and its upscale organization. This is all the more suprising when the only additional tuning that occurred on moving from a 4 km model was a reduction in the Smagorinsky mixing length.

The main deficiency in the higher resolution models was an overproduction of cloud both in an absolute sense in the diurnal cycle cloud fraction but also in the relative sense where systems had a tendency to fragment into so many small elements that they then dominated over the principle diurnal cycle at short lengthscales. The 4 km model with 3D mixing appears to ameliorate the latter somewhat but not the

former. It would be useful to run further experiments at the higher resolutions particularly running a 1.5 km model with 3D mixing and also with altered parameter values for the 4 km model with 3D mixing. However, the computational cost was sufficiently high to preclude this as part of this project.

It would be instructive to test whether the results from this case study hold more generally for other regions of the globe. Additionally, the influence of land surface structures on the initiation of convection at higher spatial resolutions would be of interest. Recent analysis by Taylor *et al.* (2011) has demonstrated the effect spatial structures in soil moisture on lengthscales of 10–40 km can have on the evolution of convection. Higher resolution models may be better able to represent these processes and their associated feedbacks.

References

Davies T, Cullen MJP, Malcolm AJ, Mawson MH, Staniforth A, White AA, Wood N. 2005. A new dynamical core for the Met Office's global and regional modelling of the atmosphere. *Q. J. R. Meteorol. Soc.* **131**: 1759–1782.

Dewitte S, Gonzalez L, Clerbaux N, Ipe A, Bertrand C, De Paepe B. 2008. The Geostationary Earth Radiation Budget Edition 1 data processing algorithms. *Advances in Space Research.* **41**.: 1906–1913.

Grabowski WW, Bechtold P, Cheng A, Forbes R, Halliwell C, Khairoutdinov M, Lang S, Nasuno T, Petch J, Tao W-K, Wong R, Wu X, Xu K-M. 2006. Daytime convective development over land: A model intercomparison based on LBA observations. *Q. J. R. Meteorol. Soc.* **132**: 317–344.

Gregory D, Rowntree PR. 1990. A mass flux convection scheme with representation of cloud ensemble characteristics and stability-dependent closure. *Mon. Wea. Rev.* **118**: 1483–1506.

Guichard F, Petch JC, Redelsperger J-L, Bechtold P, Chaboureau J-P, Cheient S, Grabowski W, Grenier H, Jones CG, Kohler M, Piriou J-M, Tailleux R, Tomasimni M. 2004. Modelling the diurnal cycle of deep precipitating convection over land with cloud-resolving models and single-column models. *Q. J. R. Meteorol. Soc.* **130**: 3139–3172.

Halliwell C. 2007. Subgrid turbulence scheme. *Unified Model Documentation Paper 28.* Met Office, Exeter, UK.

Harries JE, et al. 2005. The Geostationary Earth Radiation Budget project. *Bull. Am. Meteorol. Soc.* **86**: 945–960.

Hohenegger C, Brockhaus P, Schär C. 2008. Towards climate simulations at cloud-resolving scales. *Meteorol. Z.* **17**: 383–394.

Holloway CE, Woolnough SJ, Lister GMS. 2012. Precipitation distributions for explicit versus parametrized convection in a large-domain high-resolution tropical case study. *Q. J. R. Meteorol. Soc.* **138**: 1692–1708. DOI:10.1002/qj.1903

Kendon E, Roberts N, Senior C, Roberts M. 2012. Realism of rainfall in a very high resolution regional climate model. *J. Climate.* DOI:10.1175/JCLI-D-11-00562.1. in press.

Lean HW, Clark PA, Dixon M, Roberts NM, Fitch A, Forbes R, and Halliwell C. 2008. Characteristics of high-resolution versions of the Met Office Unified Model for forecasting convection over the United Kingdom, *Mon. Wea. Rev.* **136**: 3408–3434.

Leary CA, Houze Jr. RA. 1979. The structure and evolution of convection in a tropical cloud cluster. *J. Atmos. Sci.* **36**: 437–457.

Lock A. 2007. The parametrization of boundary layer processes. *Unified Model Documentation Paper 24.* Met Office, Exeter, UK.

Macahdo LAT, Duvel J-P, Desbois M. 1993. Diurnal variations and modulations by easterly waves of the size distribution of convective cloud clusters over west Africa and the Atlantic Ocean. *Mon. Weather Rev.* **121**: 37–49.

Marsham JH, Knippertz P, Dixon NS, Parker DJ, Lister GMS. 2011. The importance of the representation of deep convection for modeled dust-generating winds over West Africa during summer. *Geophys. Res. Lett.* **38**: L16803. DOI:10.1029/2011GL048368

Parker DJ, Fink A, Janicot S, Ngamini J-B, Douglas M, Afiesimama E, Agusti-Panareda A, Beljaars A, Dide F, Diedhiou A, Lebel T, Polcher J, Redelsperger J-L, Thorncroft C, Wilson GA., 2008. The AMMA radiosonde program and it's implications for the future of atmospheric monitoring over Africa. *Bull. Am. Meteorol. Soc.* **89**: 1015-1027. DOI:10.1175/2008BAMS2436.1

Pearson KJ, Hogan RJ, Allan RP, Lister GMS, Hollway CE. 2010. Evaluation of the model representation of convective systems using satellite observations of outgoing longwave radiation. *J. Geophys. Res.* **115**: D20206.

Randall DA *et al.* 2007. Climate models and their evaluation. in *Climate Change 2007: The Physical Science Basis. Contribution of Working Group I to the Fourth Assessment Report of the Intergovernmental Panel on Climate Change.* edited by S. Solomon et al. 589–662, Cambridge University Press, Cambridge, UK.

Roberts NM. 2003. The impact of a change to the use of the convection scheme to high-resolution simulations of convective events. *Met Office Tech. Rep. 407.* Met Office, Exeter, UK.

Staniforth A., White A., Wood N., Thuburn J., Zerroukat M., Cordero E.. Davies T., Diamantakis M. 2006. Joy of UM 6.3 - Model Formulation. *Unified Model Documentation Paper 15.* Met Office, Exeter, UK.

Stratton RA, Stirling AJ. 2011. Improving the diurnal cycle of convection in GCMs. *Q. J. R. Meteorol. Soc.* DOI:10.1002/qj.991.

Stirling AJ, Stratton RA. 2012. Entrainment processes in the diurnal cycle of deep convection over land. *Q. J. R. Meteorol. Soc.* DOI:10.1002/qj.1868.

Taylor CM, Gounou A, Guichard F, Harris PP, Ellis RJ, Couvreux F, De Kauwe M. 2011. Frequency of Sahelian storm initiation enhanced over mesoscale soil-moisture patterns. *Nature Geo.* **4**: 430–433. doi:10.1038/ngeo1173.

Yang G, Slingo J. 2001. The diurnal cycle in the tropics. *Mon. Weather Rev.* **129**: 784–801.